Atmos. Chem. Phys. Discuss., https://doi.org/10.5194/acp-2018-208
Manuscript under review for journal Atmos. Chem. Phys.
Discussion started: 13 March 2018

Atmospheric Chemistry and Physics
Discussions
Open Access

Contrasting behaviors of the atmospheric CO_2 interannual variability during two types of El Niños

Jun Wang[1,2], Ning Zeng[2,3], Meirong Wang[4], Fei Jiang[1], Jingming Chen[1,5], Pierre Friedlingstein[6], Atul K. Jain[7], Ziqiang Jiang[1], Weimin Ju[1], Sebastian Lienert[8,9], Julia Nabel[10], Stephen Sitch[11], Nicolas Viovy[12], Hengmao Wang[1], Andrew J. Wiltshire[13]

[1]International Institute for Earth System Science, Nanjing University, Nanjing, China

[2] State Key Laboratory of Numerical Modelling for Atmospheric Sciences and Geophysical Fluid Dynamics, Institute of Atmospheric Physics, Beijing, China

[3]Department of Atmospheric and Oceanic Science and Earth System Science Interdisciplinary Center, University of Maryland, College Park, Maryland, USA

[4]Joint Center for Data Assimilation Research and Applications/Key Laboratory of Meteorological Disaster of Ministry of Education, Nanjing University of Information Science & Technology, Nanjing, China

[5]Department of Geography, University of Toronto, Ontario M5S3G3, Canada

[6]College of Engineering, Mathematics and Physical Sciences, Unvernity of Exeter, Exeter EX4 4QE, UK

[7]Department of Atmosheric Sciences, University of Illinois at Urbana-Champaign, Urbana, IL 61801, USA

[8]Climate and Environmental Physics, Physics Institute, University of Bern, Bern, Switzerland

[9]Oeschger Centre for Climate Change Research, University of Bern, Bern, Switzerland

[10]Land in the Earth System, Max Planck Institute for Meteorology, D-20146 Hamburg, Germany

[11]College of Life and Environmental Sciences, University of Exeter EX4 4QF, UK

[12]Laboratoire des Sciences du Climat et de l'Environnement, LSCE/IPSL-CEA-CNRS-UVQS, F-91191, Gif sur Yvette, France

[13]Met office Hadley Centre, Fitzroy Rd, Exeter. EX1 3PB. UK

Correspondence to: (Ning Zeng, zeng@umd.edu; Fei Jiang, jiangf@nju.edu.cn)

Atmos. Chem. Phys. Discuss., https://doi.org/10.5194/acp-2018-208
Manuscript under review for journal Atmos. Chem. Phys.
Discussion started: 13 March 2018

Abstract

El Niño has two different flavors: eastern Pacific (EP) and central Pacific (CP) El Niños, with different global teleconnections. However, their different impacts on carbon cycle interannual variability remain unclear. We here compared the behaviors of the atmospheric CO_2 interannual variability and analyzed their terrestrial mechanisms during these two types of El Niños, based on Mauna Loa (MLO) CO_2 growth rate (CGR) and Dynamic Global Vegetation Models (DGVMs) historical simulations. Composite analysis shows that evolutions of MLO CGR anomaly have three clear differences in terms of (1) negative and neutral precursors in boreal spring of El Niño developing years (denoted as “yr0”), (2) strong and weak amplitudes, and (3) durations of peak from December (yr0) to April of El Niño decaying year (denoted as “yr1”) and from October (yr0) to January (yr1) during EP and CP El Niños, respectively. Models simulated global land–atmosphere carbon flux (F_{TA}) is able to capture the essentials of these characteristics. We further find that the gross primary productivity (GPP) over the tropics and extratropical southern hemisphere (Trop+SH) generally dominates the global F_{TA} variations during both El Niño types. Regionally, significant anomalous carbon uptake caused by more precipitation and colder temperature, corresponding to the negative precursor, occurs between 30°S and 20°N from January (yr0) to June (yr0), while the strongest anomalous carbon releases, due largely to the reduced GPP induced by low precipitation and warm temperature, happen between equator and 20°N from February (yr1) to August (yr1) during EP El Niño events. In contrast, during CP El Niño events, clear carbon releases exist between 10°N and 20°S from September (yr0) to September (yr1), resulted from the widespread dry and warm climate conditions. Different spatial patterns of land temperature and precipitation in different seasons associated with EP and CP El Niños

account for the characteristics in evolutions of GPP, terrestrial ecosystem respiration (TER), and resultant F_{TA}. Understanding these different behaviors of the atmospheric CO_2 interannual variability along with their terrestrial mechanisms during EP and CP El Niños is important because CP El Niño occurrence rate might increase under global warming.

1 Introduction

The El Niño–Southern Oscillation (ENSO), a dominant year-to-year climate variability, leads to a significant interannual variability in the atmospheric CO_2 growth rate (CGR) (Bacastow, 1976;Keeling et al., 1995). Many studies, including measurement campaigns (Lee et al., 1998;Feely et al., 2002), atmospheric inversions (Bousquet et al., 2000;Peylin et al., 2013), and terrestrial carbon cycle models (Zeng et al., 2005;Wang et al., 2016), consistently suggested the dominant role of terrestrial ecosystems, especially of tropical ecosystems, to the atmospheric CO_2 interannual variability. Recently, Ahlstrom et al. (2015) further suggested ecosystems over the semi-arid regions played the most important role in the interannual variability of the land CO_2 sink. Moreover, this ENSO-related carbon cycle interannual variability may be enhanced under global warming, with an about 44% increase in the sensitivity of terrestrial carbon flux to ENSO (Kim et al., 2017).

Tropical climatic variations (especially in surface air temperature and precipitation) induced by ENSO and responses of plant/soil physiology can largely account for the terrestrial carbon cycle interannual variability (Zeng et al., 2005;Wang et al., 2016;Jung et al., 2017). Multi-model simulations involved in the TRENDY project and the Coupled Model Intercomparison Project Phase 5 (CMIP5) have consistently suggested the biological dominance of the gross primary productivity (GPP) or net

Atmos. Chem. Phys. Discuss., https://doi.org/10.5194/acp-2018-208
Manuscript under review for journal Atmos. Chem. Phys.
Discussion started: 13 March 2018

primary productivity (NPP) (Kim et al., 2016;Wang et al., 2016;Piao et al., 2013;Ahlstrom et al., 2015). However, debates have continued about which is the dominant climatic mechanism (temperature or precipitation) in the interannual variability of the terrestrial carbon cycle (Wang et al., 2013;Wang et al., 2014;Cox et al., 2013;Zeng et al., 2005;Ahlstrom et al., 2015;Wang et al., 2016;Qian et al., 2008;Jung et al., 2017).

The atmospheric CGR or land–atmosphere carbon flux (F_{TA} – positive sign meaning a flux into the atmosphere) can anomalously increase during El Niño, and decrease during La Niña episodes (Zeng et al., 2005;Keeling et al., 1995). Cross correlation analysis shows that the atmospheric CGR and F_{TA} lags the ENSO by several months (Qian et al., 2008;Wang et al., 2013;Wang et al., 2016), because of the period needed for surface energy and soil moisture adjustment following ENSO-related circulation and precipitation anomalies (Gu and Adler, 2011;Qian et al., 2008). However, considering the ENSO diversity (Capotondi et al., 2015), the atmospheric CGR and F_{TA} can show different behaviors during different El Niño events (Schwalm, 2011;Wang et al., 2018).

In climate, El Niño events can be classified into eastern Pacific El Niño (EP El Niño, also termed as conventional El Niño) and central Pacific El Niño (CP El Niño, also termed as El Niño Modoki), according to the patterns of sea-surface warming over the tropical Pacific (Ashok et al., 2007;Ashok and Yamagata, 2009). These two types of El Niño have different global climatic teleconnections, associated with contrasting climate conditions in different seasons (Weng et al., 2007;Weng et al., 2009). For example, positive winter temperature anomalies are located mostly over the northeastern US during EP El Niño, while warm anomalies are in northwestern US during CP El Niño (Yu et al., 2012). The contrasting summer and winter precipitation anomaly patterns associated with these two El Niño events over the China, Japan, and US were also presented by Weng et al. (2007; 2009). Importantly, Ashok et al. (2007) suggested that the occurrence of CP El Niño had increased during recent decades, as compared to EP El Niño. This phenomenon can probably be attributed to the anthropogenic global warming (Ashok and Yamagata, 2009;Yeh et al., 2009).

However, the contrasting impacts of EP and CP El Niño events on the carbon cycle variability remain unclear. In this study, we attempt to reveal their different impacts. Therefore, we carefully compared the behaviors of the atmospheric CO_2 interannual variability and analyzed their terrestrial mechanisms corresponding to these two types of El Niños, based on Mauna Loa long-term CGR and TRENDY multi-model simulations.

This paper is organized as follows: Section 2 describes the datasets used, methods, and TRENDY models selected. Section 3 show the results about the relationship between ENSO and CGR, EP and CP El Niño events, composite analysis on carbon cycle behaviors, and terrestrial mechanisms. Some discussions will be presented in Section 4, and concluding remarks are in Section 5.

2 Datasets and Methods

2.1 Datasets used

We accessed the monthly atmospheric CO_2 concentration between 1960 and 2013 from the National Oceanic and Atmospheric Administration (NOAA) Earth System Research Laboratory (ESRL). The annual CO_2 growth rate (CGR) in Pg C yr^{-1} is derived month by month according to the approach (Patra et al., 2005;Sarmiento et al., 2010)

Atmos. Chem. Phys. Discuss., https://doi.org/10.5194/acp-2018-208
Manuscript under review for journal Atmos. Chem. Phys.
Discussion started: 13 March 2018

$$CGR(t) = \gamma \cdot [pCO_2(t+6) - pCO_2(t-6)] \quad (1)$$

where $\gamma = 2.1276$ Pg C ppm^{-1}, pCO_2 is the atmospheric partial pressure of CO_2 in ppm, t represents the time in months. The detailed calculation of the conversion factor (γ) can be referred to the appendix (Sarmiento et al., 2010).

We obtained the temperature and precipitation datasets between 1960 and 2013 from CRUNCEPv6 (Wei et al., 2014). CRUNCEP datasets are the merged product of the ground observation-based CRU data and model-based NCEP-NCAR Reanalysis data, with a 0.5°×0.5° spatial and 6 hourly temporal resolution. These datasets are consistent with the climatic forcing used to run dynamic global vegetation models in TRENDY v4 (Sitch et al., 2015). The sea surface temperature anomalies (SSTA) over the Niño3.4 region (5°S–5°N, 120°–170°W) were from the NOAA's Extended Reconstructed Sea Surface Temperature (ERSST) dataset, version 4 (Huang et al., 2015).

We also took the inversion of F_{TA} from the Jena CarboScope as a comparison with the TRENDY multi-model simulations from 1981 to 2013. The Jena CarboScope Project provides the estimates of the surface-atmosphere carbon flux based on the atmospheric measurements through an "atmospheric transport inversion". The inversion run used here is the s81_v3.8 (Rodenbeck et al., 2003).

2.2 TRENDY simulations

We analyzed eight state-of-the-art dynamic global vegetation models from TRENDY

Atmos. Chem. Phys. Discuss., https://doi.org/10.5194/acp-2018-208
Manuscript under review for journal Atmos. Chem. Phys.
Discussion started: 13 March 2018

v4 for the period 1960–2013: CLM4.5 (Oleson et al., 2013), ISAM (Jain et al., 2013), JSBACH (Reick et al., 2013), JULES (Clark et al., 2011), LPX-Bern (Keller et al., 2017), OCN (Zaehle and Friend, 2010), VEGAS (Zeng et al., 2005), and VISIT (Kato et al., 2013) (Table 1). Since LPX-Bern was excluded in the analysis of TRENDY v4, due to it not fulfilling the minimum performance requirement, the output over the same time period of a more recent version (LPX-Bern v1.3) was used. These models were forced by a common set of climatic datasets (CRUNCEPv6) and followed the same experimental protocol. The 'S3' run was used in this study, in which simulations forced by all the drivers including the CO_2, climate, and land use and land cover change (Sitch et al., 2015).

We interpolated the simulated terrestrial variables (NBP, GPP, TER, soil moisture etc.) into a consistent 0.5°×0.5° resolution using the first order conservative remapping scheme (Jones, 1999) by Climate Data Operators (CDO):

$$\overline{F_k} = \frac{1}{A_k}\int f dA \tag{2}$$

where $\overline{F_k}$ denotes the area-averaged destination quantity, A_k is the area of cell k, f is the quantity in an old grid which has overlapping area with the destination grid. Then the median, 5%, and 95% percentiles of multi-model simulations were calculated grid by grid to study the different effects of EP and CP El Niños on terrestrial carbon cycle interannual variability.

Atmos. Chem. Phys. Discuss., https://doi.org/10.5194/acp-2018-208
Manuscript under review for journal Atmos. Chem. Phys.
Discussion started: 13 March 2018

Atmospheric Chemistry and Physics
Discussions

2.3 El Niño criterion and classification methods

El Niño events are determined by the Oceanic Niño Index (ONI) [i.e. the running 3-month mean SST anomaly over the Niño3.4 region]. This NOAA criterion is that El Niño events are defined as 5 consecutive overlapping 3-month periods at or above the +0.5° anomaly.

We classified El Niño events into EP or CP based on the consensus of three different identification methods directly adopted from previous study (Yu et al., 2012). These identification methods include El Niño Modoki Index (EMI) (Ashok et al., 2007), the EP/CP-index method (Kao and Yu, 2009), and the Niño method (Yeh et al., 2009).

2.4 Anomaly calculation and composite analysis

To calculate the anomalies, we first removed the long-term climatology of the period 1960–2013 from all of the variables, in order to get rid of seasonal cycle signals. We then detrended them based on a linear regression, because (1) the trend in terrestrial carbon variables was mainly caused by long-term CO_2 fertilization and climate change, (2) the trend in CGR resulted mainly from the anthropogenic emissions. We used these detrended monthly anomalies to investigate the impacts of El Niño events on carbon cycle interannual varibility.

Specifically, we adopted the composite analysis, which is widely used in the climate research, to compare the behaviors of the carbon flux (CGR, F_{TA} i.e.) based on the selected EP and CP El Niño events. We use the Bootstrap Methods (Mudelsee, 2010) to estimate the 95% confidence intervals and the Student's t-test to estimate the significance levels in the composite analysis. The 80% significance level is selected as used in Weng et al. (2007) due to the limited EP El Niño events.

3 Results

3.1 Relationship between ENSO and atmospheric CO_2 interannual variability

The atmospheric CO_2 interannual variability closely couples with ENSO (Fig. 1), with noticeable increases during El Niño and decreases during La Niña, respectively (Bacastow, 1976;Keeling and Revelle, 1985). The correlation coefficient between MLO CGR and Niño3.4 Index from 1960 to 2013 is 0.43 ($p < 0.01$). Regression analysis further indicates that per unit increase in Nino3.4 Index can lead to 0.60 Pg C yr^{-1} increase in MLO CGR.

The variation in global F_{TA} anomaly simulated by TRENDY models resembles the MLO CGR variation, with a correlation coefficient of 0.54 ($p < 0.01$; Fig. 1b). It is close to the correlation coefficient of 0.61 ($p < 0.01$; Fig. 1b) between MLO CGR and Jena CarboScope s81 in the periods of 1981–2013. This indicates that the terrestrial carbon cycle can largely explain the atmospheric CO_2 interannual variability, as suggested by previous studies (Bousquet et al., 2000;Zeng et al., 2005;Peylin et al., 2013;Wang et al., 2016). Moreover, the correlation coefficient of TRENDY global F_{TA} and Nino3.4 Index reaches 0.49 ($p < 0.01$) and a similar regression analysis as done with the MLO CGR shows a sensitivity of 0.64 Pg C yr^{-1} K^{-1}. However, owing to the diffuse light fertilization effect induced by the eruption of Mount Pinatubo in 1991 (Mercado et al., 2009), Jena CarboScope s81 indicates that the terrestrial ecosystems have an anomalous uptake during 1991/92 El Niño event, making MLO CGR an anomalous decrease. However, TRENDY models cannot capture this phenomenon. It is not only due to a lack of a corresponding process representation in some models, but also because TRENDY protocol does not include diffuse and direct light forcing.

3.2 EP and CP El Niño events

Schematic diagrams of the two types of El Niños (EP and CP) are shown in Fig. 2. During EP El Niño events (Fig. 2a), a positive sea surface temperature anomaly (SSTA) occurs in the eastern equatorial Pacific Ocean, showing a dipole SSTA pattern with the positive zonal SST gradient. This condition forms a single cell of Walker circulation over the tropical Pacific, with the dry downdraft in the western Pacific and wet updraft in the central-eastern Pacific. In contrast, the anomalous warming in the central Pacific, sandwiched by anomalous cooling in the east and west, is observed during CP El Niño events (Fig. 2b). This tripole SSTA pattern makes the positive/negative zonal SST gradient in the western/eastern tropical Pacific, resulting in an anomalous two-cell Walker circulation over the tropical Pacific. This alteration in atmospheric circulation produces a wet region in the central Pacific. Moreover, apart from these differences in the equatorial Pacific, the SSTA in other oceanic regions also differ remarkably (Weng et al., 2007;Weng et al., 2009).

Based on the NOAA criterion, we can detect a total of 17 El Niño events from 1960 till 2013. We then categorize these events into EP or CP El Niño, relying on the consensus of three identification methods (EMI, EP/CP-index, and Niño methods)

(Yu et al., 2012). Considering the effect of diffuse radiation fertilization induced by volcano eruptions (Mercado et al., 2009), we remove the 1963/64, 1982/83, and 1991/92 El Niño events, in which Mount Agung, El Chichón, and Pinatubo erupted, respectively. Further, we closely examined those extended El Niño events (1968/70, 1976/78, 1986/88). Based on the typical responses of MLO CGR to El Niño events (anomalous increase lasting from the El Niño developing year to El Niño decaying year; Supplementary Fig. S1), we retained 1968/69, 1976/77, and 1987/88 El Niño periods. Finally, we got 4 EP El Niño and 7 CP El Niño events in this study (Table 2; Fig. 1b), with the composite SSTA evolutions in Supplementary Fig. S2.

3.3 Responses of atmospheric CGR to two types of El Niños

Based on the selected EP and CP El Niño events, we make the composite analysis with the non-smoothed detrended monthly anomalies of MLO CGR and TRENDY global F_{TA} to reveal the contrasting carbon cycle responses to these two types of El Niños (Fig. 3). Besides the differences in the location of anomalous SST warming along with the alteration of the atmospheric circulation in EP and CP El Niños shown in Fig. 2, we find that (1) different El Niño precursors: the SSTA is significant negative in EP El Niño during the boreal winter (JF) and spring (MAM) in yr0 (yr0 and yr1 refer to the El Niño developing and decaying year, respectively, hereafter), whereas the SSTA is neutral in CP El Niño; (2) different tendencies of SST ($\partial SST/\partial t$): the tendency of SST in EP El Niño is stronger than that in CP El Niño; (3) different El Niño amplitudes: due to their different tendencies of SST, the amplitude

Atmos. Chem. Phys. Discuss., https://doi.org/10.5194/acp-2018-208
Manuscript under review for journal Atmos. Chem. Phys.
Discussion started: 13 March 2018

Atmospheric Chemistry and Physics
Discussions
Open Access

of EP El Niño is basically stronger than that of CP El Niño, though they all reach maturity in November or December in yr0 (Figs. 3a and c).

Correspondingly, behaviors of MLO CGR during these two types of El Niño events also show some differences (Figs. 3b and d). During EP El Niño events (Fig. 3b), the MLO CGR is negative in boreal spring (yr0), and increases quickly from boreal fall (yr0), whereas it is neutral in boreal spring (yr0), and slowly increases from boreal summer (yr0) during CP El Niño episode (Fig. 3d). The amplitude of the MLO CGR anomaly during EP El Niño events is generally larger than that during CP El Niño events; importantly, the duration of MLO CGR peak during EP El Niño is from December (yr0) to April (yr1), while the MLO CGR anomaly peaks from October (yr0) to January (yr1) during CP El Niño. Positive MLO CGR anomaly ends around September (yr1) during both cases (Figs. 3b and d). While finalizing our paper, we noted the publication of Chylek et al. (2018) who also finds CGR amplitude difference in response to the two types of events.

Comparing the MLO CGR with the TRENDY global F_{TA} anomalies (Figs. 3b and d), we can find that TRENDY global F_{TA} can well capture the characteristics of CGR evolution during the CP El Niño. In contrast, the amplitude of the TRENDY global F_{TA} anomaly is somewhat underestimated during the EP El Niño, causing lower significance in statistics (Fig. 3b). This underestimation of global F_{TA} anomaly can, for example, be clearly seen through the comparison between the TRENDY and Jena CarboScope during the extreme 1997/98 EP El Niño (Fig. 1b). But the other characteristics can be captured. Therefore, insight into the mechanisms of these CGR evolutions during EP and CP El Niños, based on the simulations by TRENDY models, is still possible.

3.4 Regional contributions, characteristics, and their mechanisms

We separate the TRENDY global F_{TA} anomaly by major geographic regions into two parts: the extratropical northern hemisphere (NH, 23°N–90°N), and tropics plus extratropical southern hemisphere (Trop+SH, 60°S–23°N) (Fig. 4). Comparing the contributions of these two parts, we find that the F_{TA} over Trop+SH plays a more important role in global F_{TA} anomaly during both cases (Figs. 4b and d), consistent with previous studies (Bousquet et al., 2000;Peylin et al., 2013;Zeng et al., 2005;Wang et al., 2016;Ahlstrom et al., 2015;Jung et al., 2017). The F_{TA} over Trop+SH is negative in austral fall (MAM; yr0), increases from austral spring (SON; yr0), and peaks from December (yr0) to April (yr1) during EP El Niño (Fig. 4b), whereas it is nearly neutral in austral fall (yr0), increases from austral winter (JJA; yr0), and peaks from November (yr0) to March (yr1) during CP El Niño (Fig. 4d). These characteristics of evolutions in F_{TA} over Trop+SH are generally consistent with the global F_{TA} and MLO CGR (Figs. 3b and d). In contrast, the contributions from the F_{TA} anomaly over the NH are relatively weaker (or nearly neutral) (Figs. 4a and c).

According to the equation $F_{TA} = -NBP = TER - GPP + D$ (the term D represents the carbon flux caused by the disturbances such as the wildfires, harvests, grazing, land cover change etc.), the variation of F_{TA} can be explained by the variations of GPP, TER, and D. The D simulated by TRENDY is nearly neutral during both El Niño types (Fig. 4). So GPP and TER can largely account for the variation of F_{TA}. Specifically, in Trop+SH, GPP anomalies dominate the variations of F_{TA} in both El Niño types, but their evolutions differ (Figs. 4b and d). GPP anomalously increases during austral fall (yr0), and decreases from austral summer (yr1) to winter (yr1), with the minimum around April (yr1) during the EP El Niño (Fig. 4b), whereas GPP anomaly is always negative with the minimum around October or November (yr0) during the CP El Niño (Fig. 4d). The variation of TER in both El Niños is relatively weaker than that of GPP (Figs. 4b and d). The anomalous increase during austral spring (yr0) and summer (yr1) accounts for the increase in F_{TA}, and it partly cancels the decease of GPP in austral fall (yr1) and winter (yr1) during EP El Niño (Fig. 4b). In contrast, TER has a reduction in yr0 during CP El Niño (Fig. 4d). Over the NH, though F_{TA} anomaly is relatively weaker, the behaviors of GPP and TER differ in EP and CP El Niños. GPP and TER consistently decrease in the growing season of yr0 and increase in the growing season of yr1 during EP El Niño (Fig. 4a), whereas they only show some increase during boreal summer (yr1) during CP El Niño (Fig. 4c).

These evolution characteristics of GPP, TER, and resultant F_{TA} principally result from their responses to the climate variability. We present the standardized observed surface air temperature, precipitation, and TRENDY simulated soil moisture content in Fig.5. Over the Trop+SH, considering the regulation of thermodynamics and hydrological cycle on surface energy balance, variations of temperature and precipitation (soil moisture) are always opposite during the two types of El Niños (Figs. 5b and d). And adjustments of soil moisture lag precipitation for about 2–4 months, owing to the so-called 'soil memory' of water recharge (Qian et al., 2008). The variations of GPP in both El Niño types are closely associated with variations of soil moisture, namely water availability largely dominated by precipitation (Figs. 4b and d, and Figs. 5b and d), consistent with previous studies (Zeng et al., 2005;Zhang et al., 2016). Warm temperature during El Niño episodes can enhance the ecosystem respiration, but dry conditions can reduce it. These cancellations from warm and dry conditions make the amplitude of TER variation smaller than that of GPP (Figs. 4b and d). Over the NH, variations of temperature and precipitation are basically in the same direction (Figs. 5a and c), as opposed to their behaviors over the Trop+SH, because of their different climatic dynamics (Zeng et al., 2005). During the EP El Niño event, cool and dry conditions in the boreal summer (yr0) inhibit GPP and TER, whereas warm and wet conditions in the boreal spring and summer (yr1) enhance them (Fig. 5a, and Fig. 4a). In contrast, only the warm and wet condition in boreal summer (yr1) enhance GPP and TER during the CP El Niño event. (Fig. 5c and Fig. 4c). These different configurations of temperature and precipitation variations during EP and CP El Niños form the different evolution characteristics of GPP, TER, and resultant F_{TA}.

Detailed regional evolution characteristics can be seen from the hovmöller diagrams in Fig. 6 and Supplementary Figs. S3 and S4. The obvious large anomalies of F_{TA}

consistently occur from 20°N to 40°S during EP and CP El Niños (Figs. 6c and f), consistent with above analyses (Figs. 4b and d). Moreover, we can find that there is clear anomalous carbon uptake between 30°S and 20°N in the periods from January (yr0) to June (yr0) during the EP El Niño (Fig. 6c), corresponding to the negative precursor (Fig. 3b and Fig. 4b). This anomalous carbon uptake comparably comes from the three continents (Supplementary Figs. S4 a–c). Biological process analyses indicate that GPP dominates between 5°N and 20°N, and between 30°S and 15°S (Supplementary Fig. S3a), which is related to the more precipitation (Fig. 6b), while TER dominates between 15°S and 5°N (Supplementary Fig. S3b), largely due to the colder temperature (Fig. 6a). On the other hand, the strongest anomalous carbon releases occur between equator and 20°N in the periods from February (yr1) to August (yr1) during EP El Niño (Fig. 6c). The largest contribution to these anomalous carbon releases comes from the South America (Supplementary Fig. S4c), and GPP is the dominant factor to F_{TA} anomaly here (Supplementary Figs. S3a and b). Low precipitation (with a few months delayed dry conditions; Fig. 6b) and warm temperature (Fig. 6a) inhibit GPP, causing the positive F_{TA} anomaly (Fig. 6c). In contrast, the obvious carbon releases can be found between 10°N and 20°S from September (yr0) to September (yr1) during CP El Niño (Fig. 6f). More specifically, these clear carbon releases largely come from South America and tropical Asia (Supplementary Figs. S4 d–f). TER dominates between 15°S and 10°N in the periods from January (yr1) to September (yr1), and others are dominated by GPP

(Supplementary Figs. S3c and d). Widespread dry and warm conditions (Figs. 6d and e) can well explain these GPP and TER anomalies, as well as the resultant F_{TA} behavior. For more detailed information on the other regions refer to Supplementary Figs. S3 and S4.

4 Discussion

The El Niño shows large diversity in individual events (Capotondi et al., 2015), creating the large uncertainties in composite analyses (Figs. 3–5). Moreover, we only selected four EP El Niño events during the past five decades in this study, which can be used to research on the carbon cycle interannual variability (Table 1). Owing to the small samples and large inter-event spread, the statistical significance in the composite analyses will need to be further evaluated with upcoming EP El Niño events occurring in the future. However, cross-correlation analyses between long-term CGR (or F_{TA}) and Niño Index have shown that the responses of CGR (or F_{TA}) lag ENSO for a few months (Zeng et al., 2005;Wang et al., 2016;Wang et al., 2013). This phenomenon can be clearly detected in the EP El Niño composite (Fig. 3b). Therefore, composite analyses in this study can still give us some insights into the interannual variability of the global carbon cycle.

Another caveat is that TRENDY models seem to underestimate the amplitude of F_{TA} anomaly during the extreme EP El Niño events (Fig. 1b). This underestimation of F_{TA} may partly result from the bias in estimation of carbon releases induced by wildfires. As expected, the carbon releases induced by wildfires in strong El Niño events (i.e.

1997/98) played an important role in global carbon variations (van der Werf et al., 2004;Chen et al., 2017) (Supplementary Fig. S5). But, some TRENDY models (ISAM, JULES, and OCN) do not include a fire module to explicitly simulate the carbon releases induced by wildfires (Table 1), and those TRENDY models that contain a fire module generally underestimate the effects of wildfires. For instance, VISIT and JSBACH clearly underestimated the carbon flux anomaly induced by wildfires during the 1997/98 EP El Niño event (Supplementary Fig. S5).

We do not include the recent extreme 2015/16 El Niño event in this study, because the TRENDY v4 datasets cover the time span from 1860 to 2014. As shown in Wang et al. (2018), the behavior of MLO CGR in 2015/16 El Niño resembles the composite result of CP El Niño events (Fig. 3d). But the 2015/16 El Niño event had the extreme positive SSTA both over the central and eastern Pacific. Its equatorial eastern Pacific SSTA exceeded +2.0 K, comparable to the historical extreme El Niño events (e.g. 1982/83, 1997/98); the central Pacific SSTA marked the warmest event since the modern observation (https://reliefweb.int/report/world/enhancing-resilience-extreme-climate-events-lessons-2015-2016-el-ni-o-event-asia-and). Therefore, the 2015/16 El Niño event evolved not only following the EP El Niño dynamics that relied on the basin-wide thermocline variations, but also following the CP El Niño dynamics that relied on the subtropical forcing (Paek et al., 2017;Palmeiro et al., 2017). The 2015/16 extreme El Niño event can be treated as the strongest mixed EP and CP El Niño, which caused different climate anomalies compared with the extreme 1997/98 El Niño (Paek et al., 2017;Palmeiro et al., 2017) with the contrasting terrestrial and oceanic carbon cycle responses (Wang et al., 2018;Liu et al., 2017;Chatterjee et al., 2017).

Some studies (Yeh et al., 2009;Ashok and Yamagata, 2009) have suggested that CP El Niño has become or will be more frequent under global warming, compared with EP El Niño. This shift of El Niño types will alter the response patterns of terrestrial carbon cycle interannual variability, and encourage us to have further studies in the future.

5 Concluding Remarks

In this study, we investigate the different impacts of EP and CP El Niño events on the carbon cycle interannual variability in terms of the composite analysis, based on the long-term MLO CGR and TRENDY multi-model simulations. We suggest that there are three clear differences in evolutions of MLO CGR during EP and CP El Niños in terms of their precursor, amplitude, and duration of peak. Specifically, MLO CGR anomaly is negative in boreal spring (yr0) during EP El Niño events, while it is neutral during CP El Niño events; the amplitude of the CGR anomaly is generally larger during EP El Niño events than during CP El Niño events; the duration of MLO CGR peak during EP El Niño events is about from December (yr0) to April (yr1), while it peaks from October (yr0) to January (yr1) during CP El Niño events.

TRENDY multi-model simulated global F_{TA} anomalies can basically capture these characteristics. Further analysis indicates that the F_{TA} anomalies over the Trop+SH make the most contribution to the global F_{TA} anomalies during these two types of El Niño events, in which GPP anomalies generally dominate the evolutions of the F_{TA} anomalies rather than TER. Regionally, during EP El Niño events, clear anomalous carbon uptake occurs between 30°S and 20°N in the periods from January (yr0) to June (yr0), corresponding to the negative precursor, which is mainly caused by more precipitation and colder temperature. The strongest anomalous carbon releases happen between equator and 20°N in the periods from February (yr1) to August (yr1), due largely to the reduced GPP induced by low precipitation and warm temperature. In contrast, clear carbon releases exist between 10°N and 20°S from September (yr0) to September (yr1) during CP El Niño events, which are caused by the widespread dry and warm climate conditions.

Data availability. The monthly atmospheric CO_2 concentration is from NOAA/ESRL (https://www.esrl.noaa.gov/gmd/ccgg/trends/index.html). The Niño3.4 Index is from ERSST4 (http://www.cpc.ncep.noaa.gov/data/indices/ersst4.nino.mth.81-10.ascii). Temperature and precipitation are from CRUNCEP v6 (ftp://nacp.ornl.gov/synthesis/2009/frescati/temp/land_use_change/original/readme.htm). TRENDY v4 data are available from S. Sitch (s.a.sitch@exeter.ac.uk) upon your reasonable request.

Atmos. Chem. Phys. Discuss., https://doi.org/10.5194/acp-2018-208
Manuscript under review for journal Atmos. Chem. Phys.
Discussion started: 13 March 2018

Acknowledgements. We gratefully acknowledge the TRENDY DGVM community, as part of the Global Carbon Project, for access to gridded land data and the NOAA ESRL for the use of Mauna Loa atmospheric CO_2 records. This study was supported by the National Key R&D Program of China (grant no. 2017YFB0504000 and no. 2016YFA0600204), the Natural Science Foundation for Young Scientists of Jiangsu Province, China (Grant No. BK20160625), and the National Natural Science Foundation of China (Grant No. 41605039). Andrew Wiltshire was supported by the Joint UK BEIS/Defra Met Office Hadley Centre Climate Programme (GA01101).

References

Ahlstrom, A., Raupach, M. R., Schurgers, G., Smith, B., Arneth, A., Jung, M., Reichstein, M., Canadell, J. G., Friedlingstein, P., Jain, A. K., Kato, E., Poulter, B., Sitch, S., Stocker, B. D., Viovy, N., Wang, Y. P., Wiltshire, A., Zaehle, S., and Zeng, N.: The dominant role of semi-arid ecosystems in the trend and variability of the land CO_2 sink, Science, 348, 895-899, 10.1126/science.aaa1668, 2015.

Ashok, K., Behera, S. K., Rao, S. A., Weng, H., and Yamagata, T.: El Niño Modoki and its possible teleconnection, Journal of Geophysical Research, 112, 10.1029/2006jc003798, 2007.

Ashok, K., and Yamagata, T.: CLIMATE CHANGE The El Nino with a difference, Nature, 461, 481-+, 10.1038/461481a, 2009.

Bacastow, R. B.: Modulation of atmospheric carbon dioxide by the Southern Oscillation, Nature, 261, 116-118, doi:10.1038/261116a0, 1976.

Bousquet, P., Peylin, P., Ciais, P., Le Quere, C., Friedlingstein, P., and Tans, P. P.: Regional changes in carbon dioxide fluxes of land and oceans since 1980, Science, 290, 1342-1346, Doi 10.1126/Science.290.5495.1342, 2000.

Capotondi, A., Wittenberg, A. T., Newman, M., Di Lorenzo, E., Yu, J.-Y., Braconnot, P., Cole, J., Dewitte, B., Giese, B., Guilyardi, E., Jin, F.-F., Karnauskas, K., Kirtman, B., Lee, T., Schneider, N., Xue, Y., and Yeh, S.-W.: Understanding ENSO Diversity, B Am Meteorol Soc, 96, 921-938, 10.1175/bams-d-13-00117.1, 2015.

Chatterjee, A., Gierach, M. M., Sutton, A. J., Feely, R. A., Crisp, D., Eldering, A., Gunson, M. R., O'Dell, C. W., Stephens, B. B., and Schimel, D. S.: Influence of El Nino on atmospheric CO2 over the tropical Pacific Ocean: Findings from NASA's OCO-2 mission, Science, 358, 10.1126/science.aam5776, 2017.

Chen, Y., Morton, D. C., Andela, N., van der Werf, G. R., Giglio, L., and Randerson, J. T.: A pan-tropical cascade of fire driven by El Niño/Southern Oscillation, Nature Climate Change, 7, 906-911, 10.1038/s41558-017-0014-8, 2017.

Chylek, P., Tans, P., Christy, J., and Dubey, M. K.: The carbon cycle response to two El Nino types: an observational study, Environmental Research Letters, 13, 10.1088/1748-9326/aa9c5b, 2018.

Clark, D. B., Mercado, L. M., Sitch, S., Jones, C. D., Gedney, N., Best, M. J., Pryor, M., Rooney, G. G., Essery, R. L. H., Blyth, E., Boucher, O., Harding, R. J., Huntingford, C., and Cox, P. M.: The Joint UK Land Environment Simulator

(JULES), model description - Part 2: Carbon fluxes and vegetation dynamics, Geosci Model Dev, 4, 701-722, 10.5194/gmd-4-701-2011, 2011.

Cox, P. M., Pearson, D., Booth, B. B., Friedlingstein, P., Huntingford, C., Jones, C. D., and Luke, C. M.: Sensitivity of tropical carbon to climate change constrained by carbon dioxide variability, Nature, 494, 341-344, 10.1038/nature11882, 2013.

Feely, R. A., Boutin, J., Cosca, C. E., Dandonneau, Y., Etcheto, J., Inoue, H. Y., Ishii, M., Le Quere, C., Mackey, D. J., McPhaden, M., Metzl, N., Poisson, A., and Wanninkhof, R.: Seasonal and interannual variability of CO2 in the equatorial Pacific, Deep-Sea Res Pt Ii, 49, 2443-2469, Pii S0967-0645(02)00044-9, Doi 10.1016/S0967-0645(02)00044-9, 2002.

Gu, G. J., and Adler, R. F.: Precipitation and Temperature Variations on the Interannual Time Scale: Assessing the Impact of ENSO and Volcanic Eruptions, Journal of Climate, 24, 2258-2270, Doi 10.1175/2010jcli3727.1, 2011.

Huang, B., Banzon, V. F., Freeman, E., Lawrimore, J., Liu, W., Peterson, T. C., Smith, T. M., Thorne, P. W., Woodruff, S. D., and Zhang, H.-M.: Extended Reconstructed Sea Surface Temperature Version 4 (ERSST.v4). Part I: Upgrades and Intercomparisons, Journal of Climate, 28, 911-930, 10.1175/jcli-d-14-00006.1, 2015.

Jain, A. K., Meiyappan, P., Song, Y., and House, J. I.: CO2 emissions from land-use change affected more by nitrogen cycle, than by the choice of land-cover data, Global Change Biology, 19, 2893-2906, 10.1111/gcb.12207, 2013.

Jones, P. W.: First- and second-order conservative remapping schemes for grids in spherical coordinates, Mon Weather Rev, 127, 2204-2210, Doi 10.1175/1520-0493(1999)127<2204:Fasocr>2.0.Co;2, 1999.

Jung, M., Reichstein, M., Schwalm, C. R., Huntingford, C., Sitch, S., Ahlstrom, A., Arneth, A., Camps-Valls, G., Ciais, P., Friedlingstein, P., Gans, F., Ichii, K., Jain, A. K., Kato, E., Papale, D., Poulter, B., Raduly, B., Rodenbeck, C., Tramontana, G., Viovy, N., Wang, Y. P., Weber, U., Zaehle, S., and Zeng, N.: Compensatory water effects link yearly global land CO_2 sink changes to temperature, Nature, 541, 516-520, 10.1038/nature20780, 2017.

Kao, H.-Y., and Yu, J.-Y.: Contrasting Eastern-Pacific and Central-Pacific Types of ENSO, Journal of Climate, 22, 615-632, 10.1175/2008jcli2309.1, 2009.

Kato, E., Kinoshita, T., Ito, A., Kawamiya, M., and Yamagata, Y.: Evaluation of spatially explicit emission scenario of land-use change and biomass burning using a process-based biogeochemical model, Journal of Land Use Science, 8, 104-122, 10.1080/1747423x.2011.628705, 2013.

Keeling, C. D., and Revelle, R.: Effects of El-Nino Southern Oscillation on the Atmospheric Content of Carbon-Dioxide, Meteoritics, 20, 437-450, 1985.

Keeling, C. D., Whorf, T. P., Wahlen, M., and Vanderplicht, J.: Interannual Extremes in the Rate of Rise of Atmospheric Carbon-Dioxide since 1980, Nature, 375, 666-670, Doi 10.1038/375666a0, 1995.

Keller, K. M., Lienert, S., Bozbiyik, A., Stocker, T. F., Churakova, O. V., Frank, D. C.,

Atmos. Chem. Phys. Discuss., https://doi.org/10.5194/acp-2018-208
Manuscript under review for journal Atmos. Chem. Phys.
Discussion started: 13 March 2018

Klesse, S., Koven, C. D., Leuenberger, M., Riley, W. J., Saurer, M., Siegwolf, R., Weigt, R. B., and Joos, F.: 20th century changes in carbon isotopes and water-use efficiency: tree-ring-based evaluation of the CLM4.5 and LPX-Bern models, Biogeosciences, 14, 2641-2673, 10.5194/bg-14-2641-2017, 2017.

Kim, J.-S., Kug, J.-S., Yoon, J.-H., and Jeong, S.-J.: Increased Atmospheric CO2 Growth Rate during El Niño Driven by Reduced Terrestrial Productivity in the CMIP5 ESMs, Journal of Climate, 29, 8783-8805, 10.1175/jcli-d-14-00672.1, 2016.

Kim, J.-S., Kug, J.-S., and Jeong, S.-J.: Intensification of terrestrial carbon cycle related to El Niño–Southern Oscillation under greenhouse warming, Nature Communications, 8, 10.1038/s41467-017-01831-7, 2017.

Lee, K., Wanninkhof, R., Takahashi, T., Doney, S. C., and Feely, R. A.: Low interannual variability in recent oceanic uptake of atmospheric carbon dioxide, Nature, 396, 155-159, Doi 10.1038/24139, 1998.

Liu, J., Bowman, K. W., Schimel, D. S., Parazoo, N. C., Jiang, Z., Lee, M., Bloom, A. A., Wunch, D., Frankenberg, C., Sun, Y., O'Dell, C. W., Gurney, K. R., Menemenlis, D., Gierach, M., Crisp, D., and Eldering, A.: Contrasting carbon cycle responses of the tropical continents to the 2015-2016 El Nino, Science, 358, 10.1126/science.aam5690, 2017.

Mercado, L. M., Bellouin, N., Sitch, S., Boucher, O., Huntingford, C., Wild, M., and Cox, P. M.: Impact of changes in diffuse radiation on the global land carbon sink,

Atmos. Chem. Phys. Discuss., https://doi.org/10.5194/acp-2018-208
Manuscript under review for journal Atmos. Chem. Phys.
Discussion started: 13 March 2018

Atmospheric Chemistry and Physics Discussions

Nature, 458, 1014-U1087, Doi 10.1038/Nature07949, 2009.

Mudelsee, M.: Climate Time Series Analysis: Classical Statistical and Bootstrap Methods, Springer, Dordrecht, 2010.

Oleson, K., Lawrence, D., Bonan, G., Drewniak, B., Huang, M., Koven, C., Levis, S., Li, F., Riley, W., Subin, Z., Swenson, S. C., Thorne, P. W., Bozbiyik, A., Fisher, R., Heald, C., Kluzek, E., Lamarque, J. F., Lawrence, P. J., Leung, L. R., Lipscomb, W. H., Muszala, S., Ricciuto, D. M., Sacks, W. J., Tang, J., and Yang, Z.: Technical Description of version 4.5 of the Community Land Model (CLM), NCAR, 2013.

Paek, H., Yu, J.-Y., and Qian, C.: Why were the 2015/2016 and 1997/1998 extreme El Nino different?, Geophys Res Lett, 44, 10.1002/2016GL071515, 2017.

Palmeiro, F. M., Iza, M., Barriopedro, D., Calvo, N., and García-Herrera, R.: The complex behavior of El Niño winter 2015-2016, Geophys Res Lett, 44, 2902-2910, 10.1002/2017gl072920, 2017.

Patra, P. K., Maksyutov, S., Ishizawa, M., Nakazawa, T., Takahashi, T., and Ukita, J.: Interannual and decadal changes in the sea-air CO2 flux from atmospheric CO2 inverse modeling, Global Biogeochemical Cycles, 19, Artn Gb4013, Doi 10.1029/2004gb002257, 2005.

Peylin, P., Law, R. M., Gurney, K. R., Chevallier, F., Jacobson, A. R., Maki, T., Niwa, Y., Patra, P. K., Peters, W., Rayner, P. J., Rödenbeck, C., van der Laan-Luijkx, I. T., and Zhang, X.: Global atmospheric carbon budget: results from an ensemble

Atmos. Chem. Phys. Discuss., https://doi.org/10.5194/acp-2018-208
Manuscript under review for journal Atmos. Chem. Phys.
Discussion started: 13 March 2018

of atmospheric CO_2 inversions, Biogeosciences, 10, 6699-6720, 10.5194/bg-10-6699-2013, 2013.

Piao, S., Sitch, S., Ciais, P., Friedlingstein, P., Peylin, P., Wang, X., Ahlström, A., Anav, A., Canadell, J. G., Cong, N., Huntingford, C., Jung, M., Levis, S., Levy, P. E., Li, J., Lin, X., Lomas, M. R., Lu, M., Luo, Y., Ma, Y., Myneni, R. B., Poulter, B., Sun, Z., Wang, T., Viovy, N., Zaehle, S., and Zeng, N.: Evaluation of terrestrial carbon cycle models for their response to climate variability and to CO_2 trends, Global Change Biology, 2117–2132, 10.1111/gcb.12187, 2013.

Qian, H., Joseph, R., and Zeng, N.: Response of the terrestrial carbon cycle to the El Nino-Southern Oscillation, Tellus Series B-Chemical and Physical Meteorology, 60, 537-550, Doi 10.1111/J.1600-0889.2008.00360.X, 2008.

Reick, C. H., Raddatz, T., Brovkin, V., and Gayler, V.: Representation of natural and anthropogenic land cover change in MPI-ESM, J Adv Model Earth Sy, 5, 459-482, 10.1002/jame.20022, 2013.

Rodenbeck, C., Houweling, S., Gloor, M., and Heimann, M.: CO2 flux history 1982-2001 inferred from atmospheric data using a global inversion of atmospheric transport, Atmos. Chem. Phys., 3, 1919-1964, 10.5194/acp-3-1919-2003, 2003.

Sarmiento, J. L., Gloor, M., Gruber, N., Beaulieu, C., Jacobson, A. R., Fletcher, S. E. M., Pacala, S., and Rodgers, K.: Trends and regional distributions of land and ocean carbon sinks, Biogeosciences, 7, 2351-2367, 2010.

Atmos. Chem. Phys. Discuss., https://doi.org/10.5194/acp-2018-208
Manuscript under review for journal Atmos. Chem. Phys.
Discussion started: 13 March 2018

Schwalm, C. R.: Does terrestrial drought explain global CO2 flux anomalies induced by El Nino?, Biogeosciences, 8, 2493-2506, 2011.

Sitch, S., Friedlingstein, P., Gruber, N., Jones, S. D., Murray-Tortarolo, G., Ahlström, A., Doney, S. C., Graven, H., Heinze, C., Huntingford, C., Levis, S., Levy, P. E., Lomas, M., Poulter, B., Viovy, N., Zaehle, S., Zeng, N., Arneth, A., Bonan, G., Bopp, L., Canadell, J. G., Chevallier, F., Ciais, P., Ellis, R., Gloor, M., Peylin, P., Piao, S. L., Le Quéré, C., Smith, B., Zhu, Z., and Myneni, R.: Recent trends and drivers of regional sources and sinks of carbon dioxide, Biogeosciences, 12, 653-679, 10.5194/bg-12-653-2015, 2015.

van der Werf, G. R., Randerson, J. T., Collatz, G. J., Giglio, L., Kasibhatla, P. S., Arellano, A. F., Jr., Olsen, S. C., and Kasischke, E. S.: Continental-scale partitioning of fire emissions during the 1997 to 2001 El Nino/La Nina period, Science, 303, 73-76, 10.1126/science.1090753, 2004.

Wang, J., Zeng, N., and Wang, M.: Interannual variability of the atmospheric CO_2 growth rate: roles of precipitation and temperature, Biogeosciences, 13, 2339-2352, 10.5194/bg-13-2339-2016, 2016.

Wang, J., Zeng, N., Wang, M., Jiang, F., Wang, H., and Jiang, Z.: Contrasting terrestrial carbon cycle responses to the 1997/98 and 2015/16 extreme El Niño events, Earth System Dynamics, 9, 1-14, 10.5194/esd-9-1-2018, 2018.

Wang, W., Ciais, P., Nemani, R., Canadell, J. G., Piao, S., Sitch, S., White, M. A., Hashimoto, H., Milesi, C., and Myneni, R. B.: Variations in atmospheric CO_2

growth rates coupled with tropical temperature, PNAS, 110, 13061-13066, 10.1073/pnas.1314920110, 2013.

Wang, X., Piao, S., Ciais, P., Friedlingstein, P., Myneni, R. B., Cox, P., Heimann, M., Miller, J., Peng, S., Wang, T., Yang, H., and Chen, A.: A two-fold increase of carbon cycle sensitivity to tropical temperature variations, Nature, 506, 212-215, 10.1038/nature12915, 2014.

Wei, Y., Liu, S., Huntzinger, D. N., Michalak, A. M., Viovy, N., Post, W. M., Schwalm, C. R., Schaefer, K., Jacobson, A. R., Lu, C., Tian, H., Ricciuto, D. M., Cook, R. B., Mao, J., and Shi, X.: The North American Carbon Program Multi-scale Synthesis and Terrestrial Model Intercomparison Project – Part 2: Environmental driver data, Geosci Model Dev, 7, 2875-2893, 10.5194/gmd-7-2875-2014, 2014.

Weng, H., Ashok, K., Behera, S. K., Rao, S. A., and Yamagata, T.: Impacts of recent El Niño Modoki on dry/wet conditions in the Pacific rim during boreal summer, Climate Dynamics, 29, 113-129, 10.1007/s00382-007-0234-0, 2007.

Weng, H., Behera, S. K., and Yamagata, T.: Anomalous winter climate conditions in the Pacific rim during recent El Niño Modoki and El Niño events, Climate Dynamics, 32, 663-674, 10.1007/s00382-008-0394-6, 2009.

Yeh, S. W., Kug, J. S., Dewitte, B., Kwon, M. H., Kirtman, B. P., and Jin, F. F.: El Nino in a changing climate, Nature, 461, 511-514, 10.1038/nature08316, 2009.

Yu, J.-Y., Zou, Y., Kim, S. T., and Lee, T.: The changing impact of El Niño on US winter temperatures, Geophys Res Lett, 39, 10.1029/2012gl052483, 2012.

Zaehle, S., and Friend, A. D.: Carbon and nitrogen cycle dynamics in the O-CN land surface model: 1. Model description, site-scale evaluation, and sensitivity to parameter estimates, Global Biogeochemical Cycles, 24, Artn Gb1005, Doi 10.1029/2009gb003521, 2010.

Zeng, N., Mariotti, A., and Wetzel, P.: Terrestrial mechanisms of interannual CO2variability, Global Biogeochemical Cycles, 19, GB1016, 10.1029/2004gb002273, 2005.

Zhang, Y., Xiao, X., Guanter, L., Zhou, S., Ciais, P., Joiner, J., Sitch, S., Wu, X., Nabel, J., Dong, J., Kato, E., Jain, A. K., Wiltshire, A., and Stocker, B. D.: Precipitation and carbon-water coupling jointly control the interannual variability of global land gross primary production, Sci Rep, 6, 39748, 10.1038/srep39748, 2016.

Tables and Figures

Table 1 TRENDY models used in this study.

No.	models	Resolution (lat×lon)	Fire simulation	references
1	CLM4.5	0.94°×1.25°	yes	Oleson et al., 2013
2	ISAM	0.5°×0.5°	no	Jain et al., 2013
3	JSBACH	1.875°×1.875°	yes	Reick et al., 2013
4	JULES	1.6°×1.875°	no	Clark et al., 2011
5	LPX-Bern	1°×1°	yes	Keller et al., 2017
6	OCN	0.5°×0.5°	no	Zaehle et al., 2010
7	VEGAS	0.5°×0.5°	yes	Zeng et al., 2005
8	VISIT	0.5°×0.5°	yes	Kato et al., 2013

Table 2 Eastern Pacific (EP) and Central Pacific (CP) El Niño events used in this study, as identified by the majority consensus of three methods.

EP El Niño	**CP El Niño**
1972/73	1965/66
1976/77	1968/69
1997/98	1987/88
2006/07	1994/95
	2002/03
	2004/05
	2009/10

Atmos. Chem. Phys. Discuss., https://doi.org/10.5194/acp-2018-208
Manuscript under review for journal Atmos. Chem. Phys.
Discussion started: 13 March 2018

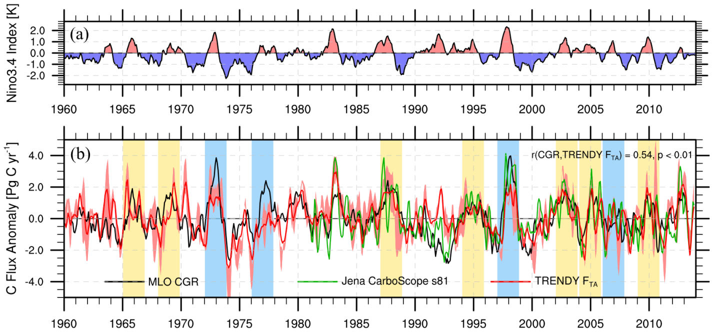

Figure 1. Interannual variability in Niño3.4 Index and carbon cycle. (a) Niño3.4. (b) Mauna Loa (MLO) CO_2 growth rate (CGR, black line), as well as TRENDY multi-model median (red line) and Jena inversion (green line) of global land–atmosphere carbon flux (F_{TA}, positive value means into the atmosphere, units in Pg C yr^{-1}), which are further smoothed by the 3-month running average. The light red shaded represents the area between the 5% and 95% percentiles of the TRENDY simulations. The bars represent the El Niño events selected in this study, with the EP El Niño in blue and CP El Niño in yellow.

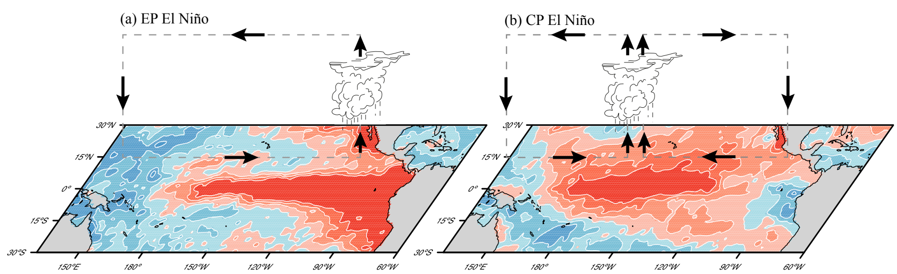

Figure 2. Schematic diagram of two types of El Niños. (a) sea surface temperature anomaly (SSTA) over the tropical Pacific associated with the anomalous Walker

Atmos. Chem. Phys. Discuss., https://doi.org/10.5194/acp-2018-208
Manuscript under review for journal Atmos. Chem. Phys.
Discussion started: 13 March 2018

Circulation in EP El Niño. (b) SSTA with two cells of the anomalous Walker Circulation in CP El Niño. Red colors indicate warming, and blue colors cooling. Vectors denote the wind directions.

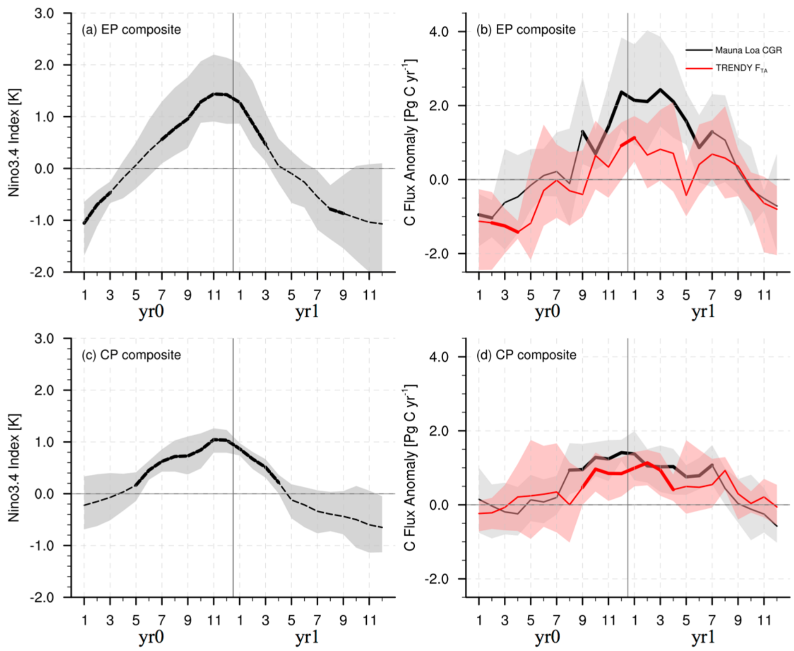

Figure 3. Composites of El Niño and corresponding carbon flux anomaly (Pg C yr^{-1}). (a) Nino3.4 Index composite during EP El Niño events. (b) corresponding MLO CGR and TRENDY v4 global F_{TA} composite during EP El Niño events. (c) Nino3.4 Index composite during CP El Niño events. (d) corresponding MLO CGR and TRENDY v4 global F_{TA} composite during CP El Niño events. Shaded area denotes the 95% confidence intervals of the variables in the composite, derived in 1000 bootstrap estimates. Bold Lines indicates the significance above the 80% level estimated by

Student's *t*-test.

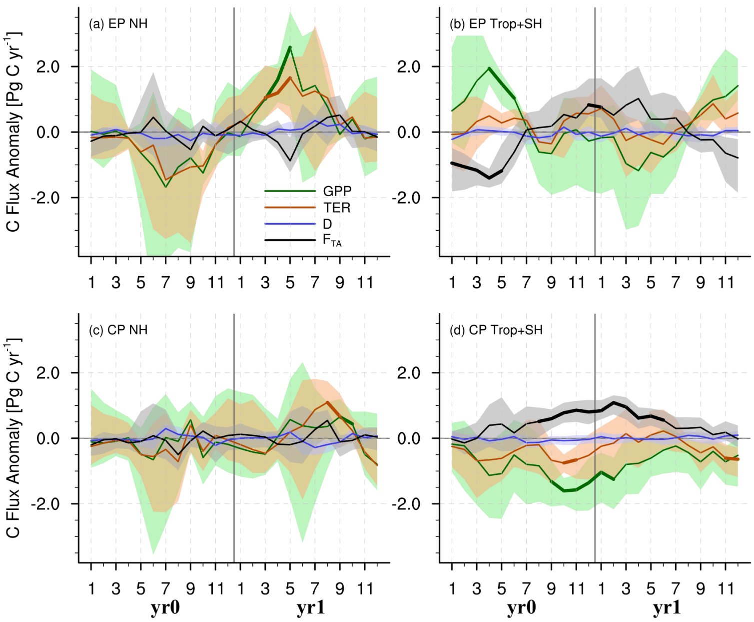

Figure 4. Composites in anomalies of the TRENDY F_{TA} (black lines), gross primary productivity (GPP, green lines), terrestrial ecosystem respiration (TER, brown lines), and the carbon flux caused by disturbances (D, blue lines) during two types of El Niños over the extratropical northern hemisphere (NH, 23°N–90°N) and the tropics and extratropical southern hemisphere (Trop+SH, 60°S–23°S). Shaded area denotes the 95% confidence intervals of the variables in the composite, derived in 1000 bootstrap estimates. Bold Lines indicates the significance above the 80% level estimated by Student's *t*-test.

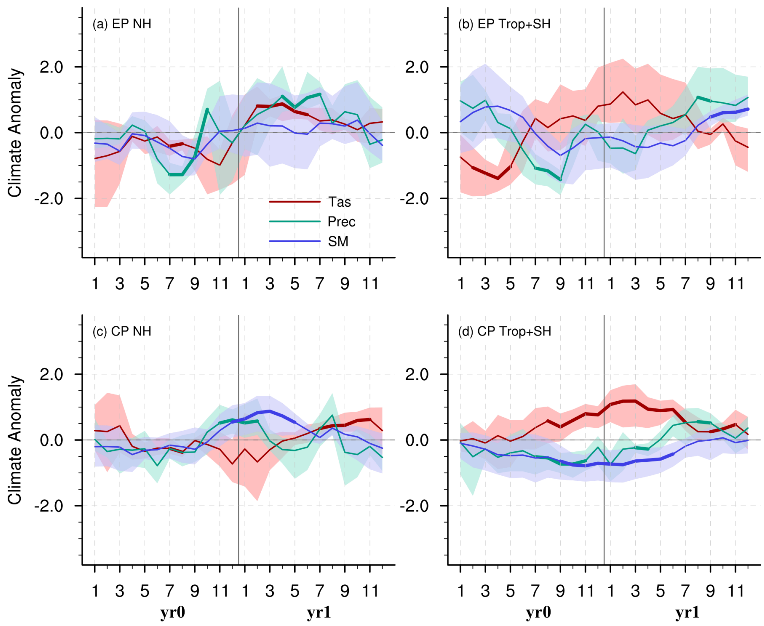

Figure 5. Composites of the standardized land surface air temperature (Tas, red lines), precipitation (green lines), and TRENDY simulated soil moisture content (SM, blue lines) anomalies in two types of El Niños over the NH, Trop+SH. Shaded area denotes the 95% confidence intervals of the variables in the composite, derived in 1000 bootstrap estimates. Bold Lines indicate the significance above the 80% level estimated by Student's *t*-test.

Atmos. Chem. Phys. Discuss., https://doi.org/10.5194/acp-2018-208
Manuscript under review for journal Atmos. Chem. Phys.
Discussion started: 13 March 2018

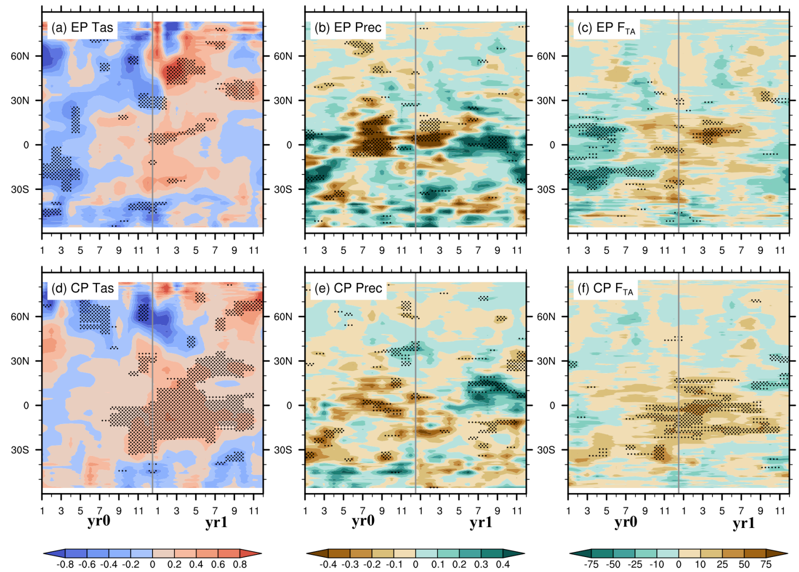

Figure 6. Hovmöller diagrams of the anomalies of climate variables and F_{TA} (averaged from 180°W to 180°E) during EP and CP El Niño events. (a and d) surface air temperature anomalies over land (units: K); (b and e) precipitation anomalies over land (units: mm d^{-1}); (c and f) TRENDY simulated F_{TA} anomalies (units: g C m^{-2} yr^{-1}) during EP and CP El Niño events, respectively. Dotted areas indicate the significance above the 80% level estimated by Student's *t*-test.